Rapid growth of organic aerosol nanoparticles over a wide tropospheric temperature range

Dominik Stolzenburg[a], Lukas Fischer[b], Alexander L. Vogel[c,d,e], Martin Heinritzi[c], Meredith Schervish[f], Mario Simon[c], Andrea C. Wagner[c], Lubna Dada[g], Lauri R. Ahonen[g], Antonio Amorim[h,i], Andrea Baccarini[e], Paulus S. Bauer[a], Bernhard Baumgartner[a], Anton Bergen[c], Federico Bianchi[g], Martin Breitenlechner[b,j,k], Sophia Brilke[a], Stephany Buenrostro Mazon[g], Dexian Chen[f], António Dias[d,h,i], Danielle C. Draper[l], Jonathan Duplissy[g], Imad El Haddad[e], Henning Finkenzeller[m], Carla Frege[e], Claudia Fuchs[e], Olga Garmash[g], Hamish Gordon[d,n], Xucheng He[g], Johanna Helm[c], Victoria Hofbauer[f], Christopher R. Hoyle[o], Changhyuk Kim[p,q], Jasper Kirkby[c,d], Jenni Kontkanen[g], Andreas Kürten[c], Janne Lampilahti[g], Michael Lawler[l], Katrianne Lehtipalo[g], Markus Leiminger[b], Huajun Mai[p], Serge Mathot[d], Bernhard Mentler[b], Ugo Molteni[e], Wei Nie[r], Tuomo Nieminen[s], John B. Nowak[t], Andrea Ojdanic[a], Antti Onnela[d], Monica Passananti[g], Tuukka Petäjä[g], Lauriane L. J. Quéléver[g], Matti P. Rissanen[g], Nina Sarnela[g], Simon Schallhart[g,u], Christian Tauber[a], António Tomé[v], Robert Wagner[g], Mingyi Wang[f], Lena Weitz[c], Daniela Wimmer[g], Mao Xiao[e], Chao Yan[f], Penglin Ye[f,t], Qiaozhi Zha[g], Urs Baltensperger[e], Joachim Curtius[c], Josef Dommen[e], Richard C. Flagan[p], Markku Kulmala[g,w], James N. Smith[l], Douglas R. Worsnop[g,t], Armin Hansel[b,x], Neil M. Donahue[f], and Paul M. Winkler[a,1]

[a]Faculty of Physics, University of Vienna, 1090 Vienna, Austria; [b]Institute for Ion Physics and Applied Physics, University of Innsbruck, 6020 Innsbruck, Austria; [c]Institute for Atmospheric and Environmental Sciences, Goethe University Frankfurt, 60438 Frankfurt am Main, Germany; [d]CERN, the European Organization for Nuclear Research, 1211 Geneva, Switzerland; [e]Laboratory of Atmospheric Chemistry, Paul Scherrer Institute, 5232 Villigen, Switzerland; [f]Center for Atmospheric Particle Studies, Carnegie Mellon University, Pittsburgh, PA 15213; [g]Institute for Atmospheric and Earth System Research/Physics, Faculty of Science, University of Helsinki, 00014 Helsinki, Finland; [h]Centro Multidisciplinar de Astrofísica, University of Lisbon, 1749-016 Lisbon, Portugal; [i]Faculdade de Ciências da Universidade de Lisboa, University of Lisbon, 1749-016 Lisbon, Portugal; [j]John A. Paulson School of Engineering and Applied Sciences, Harvard University, Cambridge, MA 02138; [k]Department of Chemistry and Chemical Biology, Harvard University, Cambridge, MA 02138; [l]Department of Chemistry, University of California, Irvine, CA 92697; [m]Department of Chemistry and Biochemistry, University of Colorado Boulder, Boulder, CO 80309; [n]School of Earth and Environment, University of Leeds, LS2 9JT Leeds, United Kingdom; [o]Institute for Atmospheric and Climate Science, ETH Zurich, 8092 Zurich, Switzerland; [p]Division of Chemistry and Chemical Engineering, California Institute of Technology, Pasadena, CA 91125; [q]Department of Environmental Engineering, Pusan National University, 46241 Busan, Republic of Korea; [r]Joint International Research Laboratory of Atmospheric and Earth System Sciences, Nanjing University, 210023 Nanjing, China; [s]Department of Applied Physics, University of Eastern Finland, 70211 Kuopio, Finland; [t]Aerodyne Research Inc., Billerica, MA 01821; [u]Finnish Meteorological Institute, 00101 Helsinki, Finland; [v]Institute Infante Dom Luíz, University of Beira Interior, 6200 Covilhã, Portugal; [w]Aerosol and Haze Laboratory, Beijing Advanced Innovation Center for Soft Matter Science and Engineering, Beijing University of Chemical Technology, Beijing, China; and [x]Ionicon Analytik GmbH, 6020 Innsbruck, Austria

Edited by John H. Seinfeld, California Institute of Technology, Pasadena, CA, and approved July 30, 2018 (received for review May 3, 2018)

Nucleation and growth of aerosol particles from atmospheric vapors constitutes a major source of global cloud condensation nuclei (CCN). The fraction of newly formed particles that reaches CCN sizes is highly sensitive to particle growth rates, especially for particle sizes <10 nm, where coagulation losses to larger aerosol particles are greatest. Recent results show that some oxidation products from biogenic volatile organic compounds are major contributors to particle formation and initial growth. However, whether oxidized organics contribute to particle growth over the broad span of tropospheric temperatures remains an open question, and quantitative mass balance for organic growth has yet to be demonstrated at any temperature. Here, in experiments performed under atmospheric conditions in the Cosmics Leaving Outdoor Droplets (CLOUD) chamber at the European Organization for Nuclear Research (CERN), we show that rapid growth of organic particles occurs over the range from −25 °C to 25 °C. The lower extent of autoxidation at reduced temperatures is compensated by the decreased volatility of all oxidized molecules. This is confirmed by particle-phase composition measurements, showing enhanced uptake of relatively less oxygenated products at cold temperatures. We can reproduce the measured growth rates using an aerosol growth model based entirely on the experimentally measured gas-phase spectra of oxidized organic molecules obtained from two complementary mass spectrometers. We show that the growth rates are sensitive to particle curvature, explaining widespread atmospheric observations that particle growth rates increase in the single-digit-nanometer size range. Our results demonstrate that organic vapors can contribute to particle growth over a wide range of tropospheric temperatures from molecular cluster sizes onward.

aerosols | nanoparticle growth | aerosol formation | CLOUD experiment | volatile organic compounds

The global budget of cloud condensation nuclei (CCN) significantly influences the Earth's radiative balance, as it affects the albedo and the lifetime of clouds. New particle formation by gas-to-particle conversion is the largest source of CCN (1). Especially the early steps of particle growth between 1 and 10 nm determine the survival chance of freshly formed particles and therefore their climatic relevance (2, 3). The major vapors driving particle growth are sulfuric acid and, maybe more importantly, low-volatility organics resulting from the oxidation of volatile organic compounds (VOCs) (4). Monoterpenes are an important class of atmospheric VOCs with copious emissions from vegetation (5). They are quickly oxidized in the atmosphere and, through a subsequent autoxidation process, rapidly

Author contributions: D.S., L.F., A.L.V., H.G., J. Kirkby, A. Onnela, U.B., J.C., J. Dommen, R.C.F., M.K., D.R.W., A.H., N.M.D., and P.M.W. designed research; D.S., L.F., A.L.V., M.H., M. Simon, A.C.W., L.D., L.R.A., A.A., A. Baccarini, P.S.B., B.B., A. Bergen, F.B., M.B., S.B., S.B.M., D.C., A.D., D.C.D., J. Duplissy, I.E.H., H.F., C. Frege, C. Fuchs, O.G., H.G., X.H., J.H., V.H., C.R.H., C.K., J. Kirkby, J. Kontkanen, A.K., J.L., M. Lawler, K.L., M. Leiminger, H.M., S.M., B.M., U.M., W.N., T.N., J.B.N., A. Ojdanic, A. Onnela, M.P., T.P., L.L.J.Q., M.P.R., N.S., S.S., C.T., A.T., R.W., M.W., L.W., D.W., M.X., C.Y., P.Y., and Q.Z. performed research; D.S., L.F., M.B., A.H., and P.M.W. contributed new reagents/analytic tools; D.S., L.F., A.L.V., M.H., M. Schervish, M. Simon, A.C.W., L.D., D.C.D., M. Lawler, R.W., L.W., and J.N.S. analyzed data; and D.S., L.F., A.L.V., M.H., J. Kirkby, N.M.D., and P.M.W. wrote the paper.

The authors declare no conflict of interest.

This article is a PNAS Direct Submission.

[1]To whom correspondence should be addressed. Email: paul.winkler@univie.ac.at.

This article contains supporting information online at www.pnas.org/lookup/suppl/doi:10.1073/pnas.1807604115/-/DCSupplemental.

Published online August 28, 2018.

Significance

Aerosol particles can form and grow by gas-to-particle conversion and eventually act as seeds for cloud droplets, influencing global climate. Volatile organic compounds emitted from plants are oxidized in the atmosphere, and the resulting products drive particle growth. We measure particle growth by oxidized biogenic vapors with a well-controlled laboratory setup over a wide range of tropospheric temperatures. While higher temperatures lead to increased reaction rates and concentrations of highly oxidized molecules, lower temperatures allow additional, but less oxidized, species to condense. We measure rapid growth over the full temperature range of our study, indicating that organics play an important role in aerosol growth throughout the troposphere. Our finding will help to sharpen the predictions of global aerosol models.

form highly oxygenated molecules (HOMs), which constitute a large source of low-volatility species in the atmosphere (6). Recent studies have shown that HOMs from the ozonolysis of the predominant monoterpene α-pinene are able to form (7) and efficiently grow particles from cluster sizes onward (8). Model simulations suggest that they are major contributors to particle formation on a global scale (9). Moreover, the impact of HOMs on initial particle growth might explain the observations of increasing growth rates with particle size between 1 and 10 nm during particle-formation events (10) by a multicomponent Kelvin effect (8, 11), also known as nano-Köhler theory (12). This is because HOMs span a wide range of volatilities (13), and, with increasing particle size, more and more low-volatility species can contribute to the growth process.

In contrast to sulfuric acid plus ammonia or amines, where growth proceeds close to the kinetic limit (14), growth driven by organics is governed by the resulting volatilities of the wide variety of oxidation products. Therefore, temperature likely plays a decisive role, as the saturation concentration has a steep exponential temperature dependence as described by the Clausius–Clapeyron relation. Additionally, a recent study has shown that temperature crucially influences the chemical composition of the initially formed molecular clusters in α-pinene ozonolysis (15). Therefore, the contribution of biogenic organics to new particle formation might be strongly sensitive to temperature. This, in turn, may significantly influence the importance of new particle formation at high altitudes (16) and in outflow regions of deep-convective clouds—for example, over the Amazon Basin (17–19).

Here, we investigate in the Cosmics Leaving Outdoor Droplets (CLOUD) chamber (20) the effect of temperature on the production of oxygenated molecules and subsequent particle growth from dark α-pinene ozonolysis at three different temperatures (-25 °C, 5 °C, and 25 °C) for various precursor concentrations. The resulting volatility distributions are inferred by combining two types of chemical ionization (CI) high-resolution time of flight mass spectrometers (TOF-MS) (21, 22) using complementary ionization techniques to obtain a detailed representation of the gaseous oxidation products. Together with the precision measurement of particle growth rates (23) and analysis of the particle-phase composition (24), this allows identification of the underlying processes and their temperature dependence responsible for initial growth in biogenic ozonolysis systems (see *Materials and Methods* for details about the experimental setup and measurement procedures).

Results

Observed Gas-Phase Composition and Volatility Distribution. We measured gas-phase composition with a nitrate-CI atmospheric pressure interface (APi)-TOF-MS (nitrate-CI) (21) and a proton transfer reaction (PTR)-TOF-MS (PTR3) (22) to obtain a more detailed overview of the neutral gas-phase species present during the α-pinene ozonolysis experiments. We obtained overlap for peaks observed in both instruments (*SI Appendix*, Fig. S3) and show a combined mass-defect plot of both instruments for three representative experiments at three different temperatures in *SI Appendix*, Fig. S4. The PTR3 introduces >200 previously undetected molecular ion signals, not only HOMs, which are usually specified by their high oxygen to carbon ratio (O:C > 0.7 for monomers), but mostly compounds toward lower oxidation states. For molecules with identified chemical composition, a volatility can be assigned according to the number of oxygen atoms n_O and the number of carbon atoms n_C within the molecule (*SI Appendix*).

As volatilities of organic compounds observed in the atmosphere vary by >10 orders of magnitude and the combined mass spectra contain ~500 different molecules, it is convenient to simplify considerations of gas-to-particle partitioning by grouping compounds together within a volatility basis set (VBS) (13, 25). Within this framework, the volatility bins are separated by one decade in C^* at 300 K, and for other temperatures, the binned distribution is shifted toward lower saturation mass concentrations. The saturation mass concentration of oxidized organics should follow the Clausius–Clapeyron relation at a constant evaporation enthalpy ΔH_{vap}, which in turn is linked to C^* at 300 K (13) (*SI Appendix*).

Fig. 1 shows the resulting binned volatility distribution of all observed organic gas-phase compounds for three representative experiments. We averaged observed gas-phase concentrations

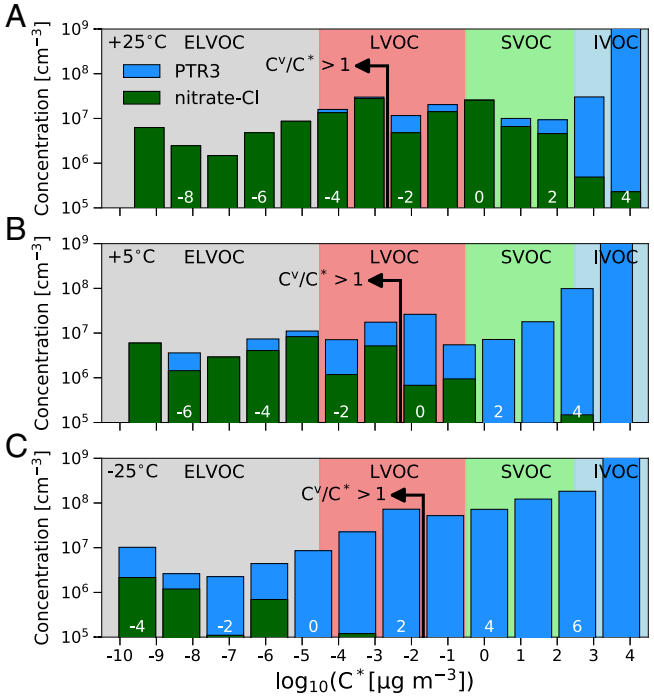

Fig. 1. Volatility distributions for representative experiments with similar α-pinene ozonolysis rate: 25 °C (*A*), 5 °C (*B*), and -25 °C (*C*). The green and blue bars show summed molecular ions observed in the nitrate-CI and PTR3, respectively. The highest and lowest bin are overflow bins. Volatility bins are defined at 300 K, shifted, and widened according to their corresponding temperature. The resulting saturation mass concentration is defined on the *x* axis, while $\log_{10} C^*_{300K}$ is specified by white numbers. Additionally, the bins in supersaturation with $C^v/C^* > 1$ are found left of the indicating arrow. ELVOC, extremely low-volatility organic compound; IVOC, intermediate-volatility organic compound; LVOC, low-volatility organic compound; SVOC, semi-volatile organic compound.

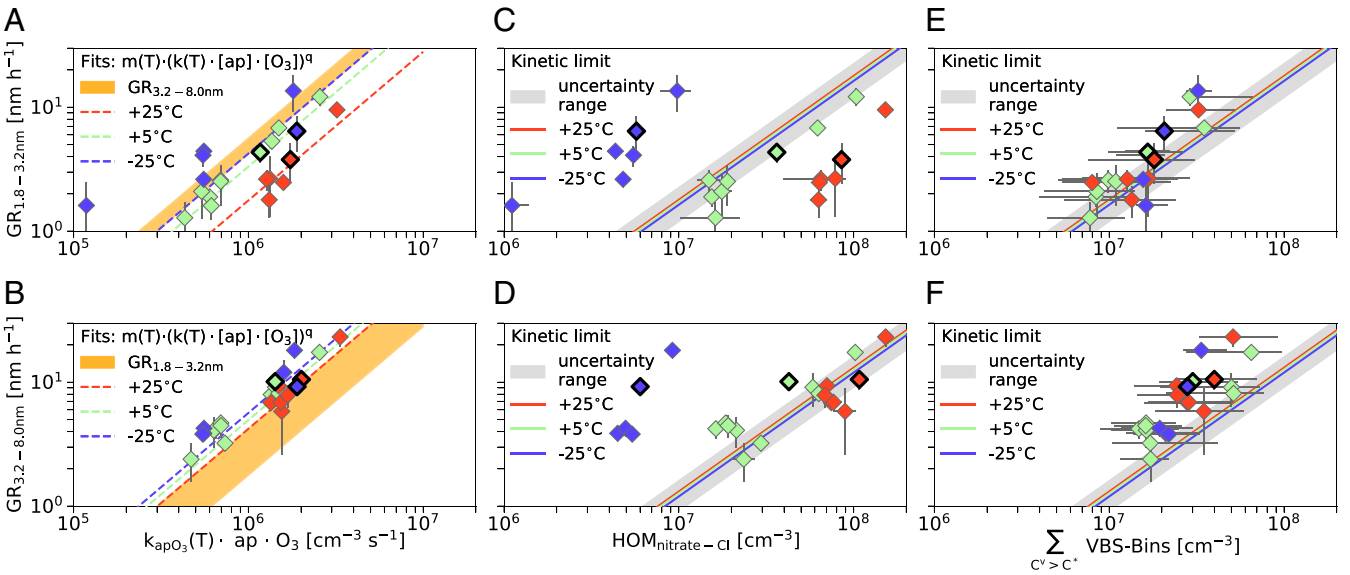

Fig. 2. Growth rates (GR) measured by the DMA train in two size intervals [1.8–3.2 nm (*A*, *C*, and *E*) and 3.2–8 nm (*B*, *D*, and *F*)] vs. several gas-phase variables. Representative experiments are highlighted. On the *x* axis, *A* and *B* show the reacted α-pinene rate, *C* and *D* show the HOMs observed in the nitrate-CI, and *E* and *F* show the amount of condensable material determined by the temperature-dependent volatility basis set. Colors in all plots indicate the run temperatures: purple corresponds to $-25\,^{\circ}$C, green to $5\,^{\circ}$C, and red to $25\,^{\circ}$C. In *A* and *B*, the light yellow areas shows the range of growth rates of the other size interval to demonstrate the observed lower growth rates at small diameters. In *C*–*F*, the gray areas illustrate the range of uncertainty on the kinetic condensation limits drawn as solid colored lines. In *E* and *F*, the error on the sum over the VBS distribution is determined from the 1-decade uncertainty in the volatility definition.

C^v over a period where comparable particle growth rates are measured with a differential mobility analyzer (DMA) train (23), and the α-pinene ozonolysis rate is similar with $\mathrm{k}(T)\cdot[\mathrm{ap}]\cdot[\mathrm{O_3}] \sim 1.4-2.0\cdot10^6$ cm^{-3}s^{-1}.

Due to the comparable growth rates of the three examples, the gas-particle partitioning is expected to be comparable, which is confirmed by the similarity of the observed total volatility distribution over the extremely low-volatility organic compound (ELVOC) and low-volatility organic compound (LVOC) ranges. Earlier work on growth of nucleated particles from α-pinene oxidation at $5\,^{\circ}$C using only a nitrate-CI found that the measured HOMs could only explain a fraction of the growth and speculated that the nitrate detection efficiency was progressively lower for less polar (and, hence, more volatile) species (8). We confirmed the missing fraction and found that the PTR3 detected many new compounds, mainly less-oxygenated molecules with $n_O \leq 7$, not measured by the nitrate-CI, independent of temperature. At low temperature, fewer polar functional groups are required for a compound to have a low volatility, and thus at $5\,^{\circ}$C, and even more significantly at $-25\,^{\circ}$C (Fig. 1 *B* and *C*, respectively), these species observed by the PTR3 contribute substantially in the LVOC and even ELVOC range.

Particle-Growth Measurements. We measured growth rates during the experiments with a DMA train over two different size intervals, 1.8–3.2 and 3.2–8 nm, by the appearance time method as it was done in comparable studies (8, 14). It gives robust apparent particle-growth rates for chamber experiments and is not affected by measurement uncertainties in absolute particle concentrations due to possible evaporation effects during the measurement procedure (*SI Appendix*). Fig. 2 shows the measured growth rates vs. several gas-phase variables. Fig. 2 *A* and *B* shows the correlation with the estimated reaction rate of the α-pinene ozonolysis during the growth rate measurement. Higher reaction rates, and hence higher product concentrations, lead to higher growth rates, following an exponential relation $m(T, d_p)\cdot(\mathrm{k}(T)\cdot[\mathrm{ap}]\cdot[\mathrm{O_3}])^q$ (*SI Appendix*). For a given α-pinene ozonolysis reaction rate, we find lower growth rates at smaller sizes. The smaller size range also shows a more significant temperature dependency: The growth rates are higher at low temperatures at a given reaction rate. This indicates that the ozonolysis products at the three different temperatures have different properties influencing their ability to condense from molecular cluster sizes onward.

Fig. 2 *C* and *D* shows the measured growth rates vs. the total HOM signal observed in the nitrate-CI only, along with a kinetic curve showing the growth rate if all measured HOMs condensed irreversibly (26). The growth rates of the three different temperatures are clearly separated, but condensation at the kinetic limit for HOMs would give almost identical values. Thus, the total HOM concentration observed in the nitrate-CI cannot fully describe the observed growth at any temperature. At $25\,^{\circ}$C, several HOMs measured by the nitrate-CI are classified as semi-volatile organic compounds and might not be able to condense, and at $-25\,^{\circ}$C, the nitrate-CI measures only a small fraction of the less-oxygenated α-pinene oxidation products responsible for particle growth (Fig. 1).

Therefore, Fig. 2 *E* and *F* shows the growth rates vs. a sum, combining both mass spectrometers, over all VBS bins in supersaturation for a given particle size—that is, with $S = K(D_p)\cdot C^v_{\mathrm{VBS\,bin}}/C^*_{\mathrm{VBS\,bin}} > 1$. A Kelvin term $K(D_p) = 10^{D_{K10}/D_p}$ accounts for the curvature of the particles, slowing growth of smaller particles. With this simple approach, it is possible to bring the growth measurements at these three different temperatures into reasonable agreement, aligning the data points roughly parallel to the kinetic line. This approach only accounts for bins in supersaturation, which should condense almost kinetically. Especially for the larger size interval, the measured growth rates were slightly higher than the supersaturated kinetic limits for all temperatures. However, some VBS bins below supersaturation will contribute as well by gas-particle partitioning, which was not considered in this simple approach.

Comparison with an Aerosol Growth Model. We modeled growth with the same framework as used in ref. 8. However, we modified the model to take real-time measured VBS distributions from both mass spectrometers as input, without any adjustments of unknown charging efficiencies (*SI Appendix*).

The most important remaining unknown in the condensation equations is the Kelvin term, $K(D_p) = 10^{D_{K10}/D_p}$, parametrized for simplicity by a decadal Kelvin diameter related to bulk liquid properties $D_{K10} = \log_{10}(e) \cdot (4\sigma M) \cdot (RT\rho)^{-1}$. However, the observed size dependence and especially the growth measurements at diameters $< D_{K10}$ should provide a direct constraint on the curvature effect. For the three representative experiments, we found the best agreement with $D_{K10}(T) = (4.8 \pm 0.8) \cdot (300\,\mathrm{K} \cdot T^{-1})$ nm. This corresponds to reasonable average properties (surface tension $\sigma = 0.03$ N·m^{-1}, molecular mass $M = 320$ g·mol^{-1}, and density $\rho = 1{,}400$ kg·m^{-3}) for the many condensing species, ignoring other possible temperature dependencies in ρ, σ, and M. Fig. 3 shows the resulting predicted growth rates and their size dependence in comparison with the measurements. The agreement between modeled and measured growth rate at the smallest sizes is within the uncertainties of the measurements. Other values for D_{K10}—for example, $D_{K10}(300K) = 3.75$ nm, used previously—lead to a significant overestimation of the observed growth rates at the smallest diameters for all temperatures. Another reason for the higher D_{K10} could be an underestimation of the volatility of the most oxygenated compounds (27). Above 5 nm, the model agreed well with the observations at all temperatures. Considering the 1-decade uncertainty in saturation mass concentration (*SI Appendix*), we achieved reasonable mass balance for growth of freshly nucleated particles between 2 and 30 nm over a wide range of conditions.

Although there was no disagreement of the model with the measurements, within the uncertainties, there are several contributions that we have not considered. First, some condensable compounds might still be undetected by the two used ionization chemistries. Additionally, fragmentation of molecules within the instruments might disturb the volatility estimate. Second, the temperature dependence of organic volatilities is also subject to uncertainties (13). Third, we did not model any particle-phase reactions, such as oligomerization. Reactive uptake is thought to be more important at larger particle sizes (28), again in part because of the Kelvin effect (29).

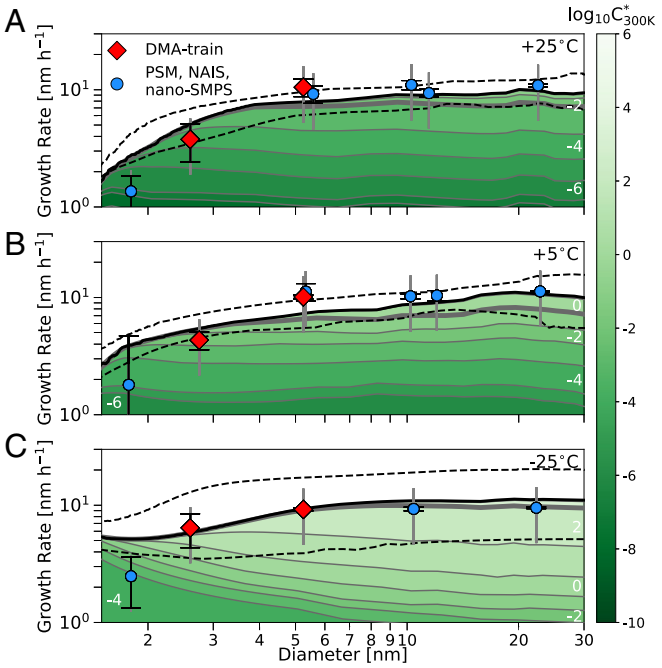

Fig. 3. Modeled and measured growth rate vs. particle diameter. (*A*) Shown is 25 °C at increasing α-pinene ozonolysis reaction rates ($\sim 1.7 - 2.3 \cdot 10^6$ cm^{-3}s^{-1}). (*B*) Shown is 5 °C at increasing reaction rates ($\sim 1.2 - 1.8 \cdot 10^6$ cm^{-3}s^{-1}). (*C*) Shown is −25 °C at constant reaction rates ($\sim 1.9 \cdot 10^6$ cm^{-3}s^{-1}). The thick black lines indicate the modeled total growth rate inferred from real-time oxidized organics measurements, and the dashed black lines indicate the associated uncertainty resulting from a ±1 bin shift of the VBS distribution. The contribution of the different bins of the VBS distribution is illustrated by the colored areas, where white numbers and the color code represent the saturation mass concentration at 300 K for all three cases. The contribution below the thick gray line is from bins with $C^v > C^*$. For the measured growth rates, red diamonds show the DMA train (shown as well in Fig. 2) and blue circles show other instruments: the neutral cluster and air ion spectrometer (NAIS), the nanoscanning mobility particle sizer (nano-SMPS), and the particle-size magnifier (PSM) (*SI Appendix*). The capped black error bar shows the statistical uncertainty of the single measurements, while the gray error bar gives the 50% systematic uncertainty of the appearance time method.

Particle-Phase Composition Measurements. The predictions by the aerosol growth model were supported by the measurement of the particle-phase composition using a filter inlet for gas and aerosols (FIGAERO) (24) attached to a O_2^--CI-APi-TOF-MS [FIGAERO-chemical ionization mass spectrometer (CIMS)] (*SI Appendix*). Fig. 4 shows the desorption profiles of three molecular ion signals corresponding to $C_{10}H_{16}O_4$, $C_{10}H_{16}O_6$, and $C_{10}H_{16}O_9$. We accumulated particles on the FIGAERO filter inlet at chamber temperature during the three experiments at −25 °C, 5 °C, and 25 °C. The signal intensity was normalized to the accumulated mass on the filter inferred from the measured particle-size distributions and sample flow rate, which allowed for quantitative comparison of the three temperatures. We fit the desorption profiles with a bimodal distribution, where the first mode represented the monomer signal and the second mode was due to fragmentation products of less volatile dimers which therefore desorb at higher temperatures (*SI Appendix*). Desorption of the monomer clearly occurred earlier for the less-oxygenated products, which experimentally confirmed the volatility dependence on n_O used for the volatility estimates.

It was evident that the less-oxygenated monomers only appeared at lower temperature in the particle phase. $C_{10}H_{16}O_4$ contributed significantly only at −25 °C, and $C_{10}H_{16}O_6$ appeared already at 5 °C in the particle phase. For $C_{10}H_{16}O_9$, a subsequent reduction in the normalized particle-phase intensity was observed for decreasing temperatures. Although the volatility of this molecule is low enough to contribute significantly even at 25 °C, its production in the gas phase was reduced at lower temperatures, and its contribution to the particle phase thus decreased with decreasing temperature.

These trends are supported by the comparison of gas- and particle-phase composition within the representative $C_{10}H_{16}O_{3-9}$ series, which contains the most dominant peaks of the particle-phase mass spectra. In Fig. 5, the fractional contributions of $C_{10}H_{16}O_{3-9}$ are shown for the gas and particle phase for the three investigated temperatures. Generally, the most abundant gas-phase product at all temperatures within this series is pinonic acid ($C_{10}H_{16}O_3$), having a similar yield to all HOM products together (7, 30). However, the fraction of the contribution of highly oxygenated products increased significantly at warmer temperatures (see also *SI Appendix*, Fig. S4), while at −25 °C, less oxygenated products dominated the gas phase completely. In the particle phase, HOM products were mainly found at 25 °C, while at lower temperatures, the particle phase contained a large contribution of less-oxygenated molecules with even a strong contribution of the modestly oxygenated pinonic

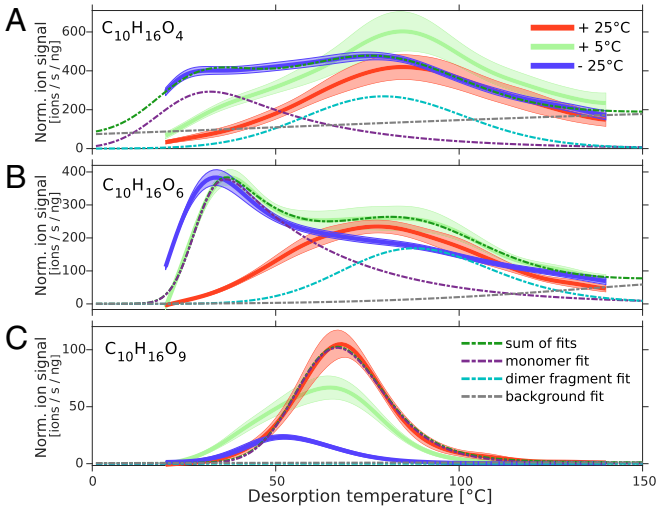

Fig. 4. Mean thermal desorption profile of three compounds found in particle-phase composition measurements with a FIGAERO-CIMS and the corresponding SE (shaded areas). The signal intensity normalized (Norm.) by primary ion signal and collected particle mass vs. the desorption temperature is compared for three representative experiments with red indicating 25 °C, green indicating 5 °C, and dark blue indicating −25 °C. For all three temperatures, the mean of the median mass diameters during sampling was between 40 and 50 nm, which should be representative for sizes $\gg D_{K10}$. *A* shows the desorption profiles of $C_{10}H_{16}O_4$, *B* of $C_{10}H_{16}O_6$, and *C* of $C_{10}H_{16}O_9$. Fits for the monomer, dimer fragment, and background signal are indicated for a single temperature on each profile.

acid. This is not only because of the decrease of the availability of gas-phase HOM products, but mainly due to a strong drop in volatility of all compounds, resulting in condensation of lower-oxygenated products. This is similar to the observations in ref. 15, where a significant decrease in O:C of the nucleating charged clusters was observed at colder temperatures.

Conclusion

Organics play a leading role in atmospheric new particle formation and growth and thus govern the global budget of CCN. VOC oxidation products in the atmosphere make up a substantial portion of condensing vapors causing growth of existing particles. Because oxidized organics span a wide range of volatilities, temperature is a crucial parameter. We use a combination of mass spectrometers, two using complementary ionization techniques for gas-phase measurements and one measuring particle-phase composition. Consideration of the volatility distribution of the measured gas-phase compounds, here with a volatility basis set, gives a sufficient constraint of the gas-phase products to comprehensively describe growth over a wide temperature range. The measured and modeled particle-phase compositions are self-consistent. The measurements are in good agreement with an aerosol growth model, and a direct estimate of the Kelvin diameter for organics of (4.8 ± 0.8) nm at 300 K could be inferred.

Temperature influences the growth by organics from dark α-pinene ozonolysis in several ways via competing processes. At higher temperatures, the increasing extent of autoxidation leads to high yields of highly oxygenated products in the gas phase. This is due to the temperature dependence of the unimolecular autoxidation reactions. It is highly likely that the intramolecular H-atom transfer reactions have significantly higher activation energies than radical–radical termination reactions, and so it is reasonable that the extent of autoxidation will increase with increasing temperature (31). On the other hand, the strong drop in volatility leads to significant condensation of less-oxygenated molecules at lower temperatures. Our precision measurements of particle-growth rates across the critical size range from 2 to 30 nm reveals that organic condensation drives particle growth at a similar rate over a wide temperature range, when the precursor oxidation rate is held constant. The temperature-dependent effects illustrated in Fig. 5 are thus of the same order of magnitude: Less extensive oxygenation at lower temperature is counterbalanced by lower volatility. This suggests a crucial role of organics in aerosol growth across the wide temperature range of the troposphere. Not only due to higher emission and ozonolysis reaction rates, but also due to rapid autoxidation to highly oxygenated products, organics can influence aerosol growth dramatically in warm regions. However, due to the strong drop in volatility of modestly oxygenated organic products, such compounds can drive aerosol growth at low temperatures. This observation could be of special interest for regions with high biogenic emissions (e.g., the Amazon basin), where compounds like pinonic acid could dominate early aerosol growth at low temperatures after convective updraft (32). Global aerosol models therefore need to implement robust descriptions of these processes, not only considering the first-order rate constants of ozonolysis and OH reactivity, but, rather, a more detailed description of organic chemistry and its temperature dependence. Precision measurements with a complementary set of mass spectrometers and particle-size-distribution measurements in the crucial region of <10 nm provide important constraints for model predictions of the contribution of gas-to-particle conversion to the global budget of CCN.

Materials and Methods

The CERN, the European Organization for Nuclear Research, CLOUD chamber is a 26.1-m^3 electropolished stainless-steel vessel, surrounded by a thermal housing capable of stabilizing temperature in a range from −65 °C to 100 °C with ±0.1 K precision (33). The chamber is equipped with a gas-control system achieving extremely high purities by mixing boil-off nitrogen and boil-off oxygen at the atmospheric ratio of 79:21. Highly pure trace gases can be precisely added at the parts per trillion (ppt) level. Before the experiments, the chamber was heated to 100 °C and rinsed with ultrapure water. This assured operation at contaminant levels of $<5 \times 10^4$ cm^{-3} H_2SO_4 and total organics <150 ppt by volume (15, 20).

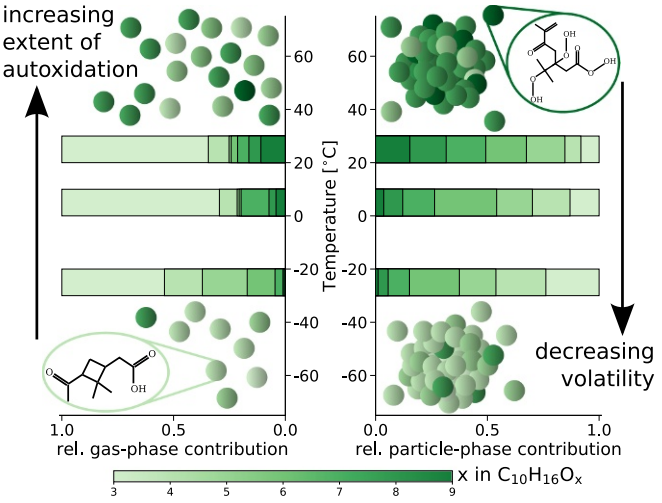

Fig. 5. Overview of the competing processes and their temperature dependence and comparison between the relative (rel.) gas- and particle-phase contribution of the ozonolysis product group $C_{10}H_{16}O_{3-9}$. *Left* shows the normalized relative contribution of the different oxygenated molecules within the gas phase, while *Right* shows the normalized relative contribution of the same compounds within the particle phase, inferred from monomer desorption fits.

Experiments were conducted as follows: At 38% relative humidity, with no SO_2 and no NO_x present in the chamber, stable ozone concentrations of 30–40 parts per billion were established. Under dark conditions (i.e., without any additional OH radical production mechanism except from the ozonolysis itself), a high-voltage field cage inside the chamber was switched on to perform neutral experiments first. Injection of α-pinene initiated the ozonolysis reaction and the subsequent formation of particles. After steady-state α-pinene concentrations were reached and particle growth was measured up to at least 10 nm, the high-voltage field was switched off. Ions now present in the chamber led to a significant increase in nucleation rate (7). Therefore, two growth rate measurements could eventually be performed, as the size distribution will show two growing particle populations. The second measurement was independent of changing gas concentrations, as steady-state was reached during the neutral stage. As no significant effect on growth due to different ionization levels was found, all measurements are treated equally.

The key particle-size distribution and growth-rate measurements of this study were performed with a DMA train (23). The sheath flows of the six DMAs were conditioned to chamber temperature to avoid possible particle evaporation during particle sizing. A 50% systematic uncertainty was assumed on the apparent particle-growth rates inferred by the appearance time method when comparing the values to growth rates from pure condensation. This also covered uncertainties of possible evaporation during the measurement procedure. Details can be found in *SI Appendix*. Gas-phase composition was measured by two complementary mass spectrometers using different ionization techniques (21, 22). For molecular ion signals observed in both instruments, the stronger signal was used to account for a reduced charging efficiency by any of the two ionization chemistries. For more details, see *SI Appendix*. Particle-phase composition was measured with a FIGAERO-CIMS (24), which accumulated particles for 30 min on a filter inlet kept at chamber temperature. As all experiments were started with a particle-free chamber, all collected particles originated from new particle formation under similar experimental conditions. The accumulated particles were thermally desorbed by heating the filter, and their composition was analyzed by the connected mass spectrometer. Details can be found in *SI Appendix*.

ACKNOWLEDGMENTS. We thank T. Kurten and N. Hyttinen for providing helpful COSMOtherm volatility estimates. We also thank K. Ivanova, P. Carrie, L.-P. De Menezes, J. Dumollard, F. Josa, I. Krasin, R. Kristic, A. Laassiri, O. S. Maksumov, B. Marichy, H. Martinati, S. V. Mizin, R. Sitals, A. Wasem, and M. Wilhelmsson for their contributions to the experiment. We thank the European Organization for Nuclear Research (CERN) for supporting CLOUD with important technical and financial resources and for providing a particle beam from the CERN Proton Synchrotron. This research was supported by the European Commission Seventh Framework Programme (Marie Curie Initial Training Network "CLOUD-TRAIN" 316662); German Federal Ministry of Education and Research Grants 01LK1222 A and 01LK1601 A; Swiss National Science Foundation Projects 20FI20_159851, 200020_172602, and 20FI20_172622; Austrian Research Funding Association FFG Project 846050; Austrian Science Fund (FWF) Projects J3951-N36 and J-3900; European Research Council (ERC) Consolidator Grant NANO-DYNAMITE 616075; ERC-Advanced Grant DAMOCLES 692891; ERC Starting Grant COALA 638703; Horizon 2020 Marie Sklodowska-Curie Grant 656994 ("Nano-CAVa"); ERC Advanced Grant 742206 ATM-GP; Academy of Finland Center of Excellence Programme Grant 307331; US Department of Energy Grant DE-SC0014469; and the Presidium of the Russian Academy of Sciences Program "High Energy Physics and Neutrino Astrophysics" 2015.

1. Gordon H, et al. (2017) Causes and importance of new particle formation in the present-day and preindustrial atmospheres. *J Geophys Res Atmos* 122:8739–8760.
2. Lehtinen KE, Maso MD, Kulmala M, Kerminen VM (2007) Estimating nucleation rates from apparent particle formation rates and vice versa: Revised formulation of the Kerminen–Kulmala equation. *J Aerosol Sci* 38:988–994.
3. Pierce JR, Adams PJ (2007) Efficiency of cloud condensation nuclei formation from ultrafine particles. *Atmos Chem Phys* 7:1367–1379.
4. Riipinen I, et al. (2012) The contribution of organics to atmospheric nanoparticle growth. *Nat Geosci* 5:453–458.
5. Guenther AB, et al. (2012) The model of emissions of gases and aerosols from nature version 2.1 (Megan2.1): An extended and updated framework for modeling biogenic emissions. *Geosci Model Dev* 5:1471–1492.
6. Ehn M, et al. (2014) A large source of low-volatility secondary organic aerosol. *Nature* 506:476–479.
7. Kirkby J, et al. (2016) Ion-induced nucleation of pure biogenic particles. *Nature* 533:521–526.
8. Tröstl J, et al. (2016) The role of low-volatility organic compounds in initial particle growth in the atmosphere. *Nature* 533:527–531.
9. Gordon H, et al. (2016) Reduced anthropogenic aerosol radiative forcing caused by biogenic new particle formation. *Proc Natl Acad Sci USA* 113:12053–12058.
10. Kulmala M, et al. (2013) Direct observations of atmospheric aerosol nucleation. *Science* 339:943–946.
11. Donahue NM, Trump ER, Pierce JR, Riipinen I (2011) Theoretical constraints on pure vapor-pressure driven condensation of organics to ultrafine particles. *Geophys Res Lett* 38:L16801.
12. Kulmala M, Kerminen VM, Anttila T, Laaksonen A, O'Dowd CD (2004) Organic aerosol formation via sulphate cluster activation. *J Geophys Res Atmos* 109:D04205.
13. Donahue NM, Epstein SA, Pandis SN, Robinson AL (2011) A two-dimensional volatility basis set: 1. Organic-aerosol mixing thermodynamics. *Atmos Chem Phys* 11:3303–3318.
14. Lehtipalo K, et al. (2016) The effect of acid–base clustering and ions on the growth of atmospheric nano-particles. *Nat Commun* 7:11594.
15. Frege C, et al. (2018) Influence of temperature on the molecular composition of ions and charged clusters during pure biogenic nucleation. *Atmos Chem Phys* 18: 65–79.
16. Bianchi F, et al. (2016) New particle formation in the free troposphere: A question of chemistry and timing. *Science* 352:1109–1112.
17. Murphy BN, Julin J, Riipinen I, Ekman AML (2015) Organic aerosol processing in tropical deep convective clouds: Development of a new model (CRM-ORG) and implications for sources of particle number. *J Geophys Res Atmos* 120:10,441–10,464.
18. Wang J, et al. (2016) Amazon boundary layer aerosol concentration sustained by vertical transport during rainfall. *Nature* 539:416–419.
19. Andreae MO, et al. (2018) Aerosol characteristics and particle production in the upper troposphere over the Amazon basin. *Atmos Chem Phys* 18:921–961.
20. Kirkby J, et al. (2011) Role of sulphuric acid, ammonia and galactic cosmic rays in atmospheric aerosol nucleation. *Nature* 476:429–433.
21. Jokinen T, et al. (2012) Atmospheric sulphuric acid and neutral cluster measurements using CI-APi-TOF. *Atmos Chem Phys* 12:4117–4125.
22. Breitenlechner M, et al. (2017) PTR3: An instrument for studying the lifecycle of reactive organic carbon in the atmosphere. *Anal Chem* 89:5824–5831.
23. Stolzenburg D, Steiner G, Winkler PM (2017) A DMA-train for precision measurement of sub-10 nm aerosol dynamics. *Atmos Meas Tech* 10:1639–1651.
24. Lopez-Hilfiker FD, et al. (2014) A novel method for online analysis of gas and particle composition: Description and evaluation of a filter inlet for gases and AEROsols (FIGAERO). *Atmos Meas Tech* 7:983–1001.
25. Donahue NM, Robinson AL, Stanier CO, Pandis SN (2006) Coupled partitioning, dilution, and chemical aging of semivolatile organics. *Environ Sci Technol* 40:2635–2643.
26. Nieminen T, Lehtinen KEJ, Kulmala M (2010) Sub-10 nm particle growth by vapor condensation–Effects of vapor molecule size and particle thermal speed. *Atmos Chem Phys* 10:9773–9779.
27. Kurtén T, et al. (2016) Alpha-pinene autoxidation products may not have extremely low saturation vapor pressures despite high O: C ratios. *J Phys Chem A* 120:2569–2582.
28. Apsokardu MJ, Johnston MV (2018) Nanoparticle growth by particle-phase chemistry. *Atmos Chem Phys* 18:1895–1907.
29. Chuang WK, Donahue NM (2017) Dynamic consideration of smog chamber experiments. *Atmos Chem Phys* 17:10019–10036.
30. Yu J, Cocker DR, Griffin RJ, Flagan RC, Seinfeld JH (1999) Gas-phase ozone oxidation of monoterpenes: Gaseous and particulate products. *J Atmos Chem* 34:207–258.
31. Praske E, et al. (2018) Atmospheric autoxidation is increasingly important in urban and suburban North America. *Proc Natl Acad Sci USA* 115:64–69.
32. Topping D, Connolly P, McFiggans G (2013) Cloud droplet number enhanced by co-condensation of organic vapours. *Nat Geosci* 6:443–446.
33. Dias A, et al. (2017) Temperature uniformity in the CERN CLOUD chamber. *Atmos Meas Tech* 10:5075–5088.